

Fast multiqubit Rydberg geometric fan-out gates with optimal control technologyJ.-F. Wei,¹ F.-Q. Guo,¹ D.-Y. Wang,¹ Y. Jia,^{2,1} L.-L. Yan^{⊗,1,*}, M. Feng,^{3,1,4,†} and S.-L. Su^{⊗,1,‡}¹*School of Physics, Key Laboratory of Materials Physics of Ministry of Education, and International Laboratory for Quantum Functional Materials of Henan, Zhengzhou University, Zhengzhou 450001, China*²*Key Laboratory for Special Functional Materials of Ministry of Education and School of Materials and Engineering, Henan University, Kaifeng 475001, China*³*State Key Laboratory of Magnetic Resonance and Atomic and Molecular Physics, Wuhan Institute of Physics and Mathematics, Innovation Academy of Precision Measurement Science and Technology, Chinese Academy of Sciences, Wuhan 430071, China*⁴*Research Center for Quantum Precision Measurement, Guangzhou Institute of Industry Technology, Guangzhou 511458, China*

(Received 25 October 2021; revised 12 February 2022; accepted 22 March 2022; published 4 April 2022)

Practical quantum computation requires highly efficient implementation of quantum logic gates. The fan-out gate represents such a type of multiqubit controlled gate with one qubit controlling a number of target qubits. Recent efforts for fan-out gates using Rydberg atoms include adiabatic operations along with the dark-state dynamics of Rydberg states [M. Khazali and K. Mølmer, *Phys. Rev. X* **10**, 021054 (2020)] and implementation based on the asymmetric Rydberg-Rydberg interaction [J. T. Young *et al.*, *Phys. Rev. Lett.* **127**, 120501 (2021)]. Inspired by these advances, we propose a fast-operation scheme for geometric multiqubit fan-out gates, in which the target qubits can be executed with arbitrary operations based on the asymmetric Rydberg-Rydberg interaction and time-optimal control technology. One of the main favorable features of our scheme is its performance in a nonadiabatic way and with the time-optimal control technology, by which the shortest smooth geometric path is found. Another feature, that the target qubits could be executed with arbitrary geometric quantum operations, makes our scheme general and useful. Therefore, our scheme provides a promising alternative route toward scalable fault-tolerant quantum information processing based on Rydberg atoms.

DOI: [10.1103/PhysRevA.105.042404](https://doi.org/10.1103/PhysRevA.105.042404)**I. INTRODUCTION**

Rydberg atoms are a kind of neutral atom subject to dipole-dipole interaction when excited to high-lying Rydberg states [1–7]. This dipole-moment-induced interaction, called Rydberg-Rydberg interaction (RRI), can give rise to a Rydberg blockade [8–11], in which one atom excited to the Rydberg state prohibits the adjacent atoms from being excited to their Rydberg state and thus provides a way to fast quantum logic gating [8,11–15]. So far, universal quantum computation with neutral atoms is in principle available. Single-qubit operations have been well studied experimentally [15], even with high fidelity [16–20]. Quantum controls [21] were also demonstrated in neutral atoms, where two-qubit gates based on RRI have been carried out experimentally [22–29].

Multiqubit gates are efficient and also versatile [30–37] and can be applied to expedite conspicuously quantum algorithms [38–41], quantum error correction [42–44], and state preparation [45]. Many previous approaches for multiqubit Rydberg gates relied on asymmetric Rydberg blockade induced by spatial asymmetry, which is usually complicated by scale differences between different types of Rydberg interactions [30,36,46–49]. By choosing an interatomic distance D , strong $1/D^3$ dipole-dipole interactions and weaker $1/D^6$

van der Waals (vdW) interactions have been acquired [47]. In contrast to changing the distance between atoms to achieve such an interaction induced by spatial asymmetry, a variety of approaches have recently been proposed to modify Rydberg interactions using microwave fields [48–59]. Of these two methods to realize an asymmetric Rydberg blockade, the former depends more on spatial asymmetry whereas the latter depends on dispersion coefficients. Additionally, researchers have recently proposed different ways to constitute multiqubit Rydberg gates, such as adiabatic operations along Rydberg excited dark eigenstates [60] and unconventional Rydberg pumping closely related to the ground states of the atoms [61]. These multiqubit gates, however, are only for specific phase operations on target qubits and also are extremely fragile due to the inevitable interaction with the surrounding environment. This motivates us to construct the multiqubit gates with arbitrary operations on the target atoms with higher fidelity and stronger robustness.

Quantum gates using geometric phases, due to their built-in noise-resilience features, are promising strategies for robust quantum computation [62–64]. Explicitly, geometric quantum computation [65–68] has been proposed through the adiabatic geometric phases, including the adiabatic Abelian geometric phase [69] and adiabatic non-Abelian geometric phase [70]. However, the adiabatic condition implies a lengthy gating time; thus the environment-induced decoherence would cause considerable gate infidelity. To overcome such limitations, nonadiabatic geometric quantum computation [71–74] based on nonadiabatic Abelian geometric phases [75] and

*llyan@zzu.edu.cn

†mangfeng@wipm.ac.cn

‡slsu@zzu.edu.cn

nonadiabatic holonomic quantum computation (NHQC) [76,77] based on nonadiabatic non-Abelian geometric phases [78] have been proposed. In particular, nonadiabatic holonomic quantum computation [76,77] employs the holonomic matrix itself as a quantum gate, which makes the NHQC possess a whole geometric property depending only on the global properties of evolution paths and not on the concrete details. Due to the merits of both geometric robustness and high-speed implementation without the limit of adiabatic evolution, NHQC has received considerable attention and was extended to further enhancing gate fidelity [79–87]. However, the implementation of NHQC is sensitive to imperfect operations and also the implementation time is unnecessarily long for most of the geometric gates, especially for the gates with small rotation angles.

In this paper we propose a fast and reliable scheme to implement the high-fidelity geometric fan-out gate based on unconventional geometric phases, NHQC, and asymmetric blockade, in which the operation time is independent of the qubit number and the fan-out gate executes arbitrary operations on the target qubits. Recent works on NHQC and neutral atoms provide solid theoretical support, and our scheme is experimentally relevant since our consideration of the Rydberg blockade regime has been fully witnessed experimentally [29,81,88–92]. In particular, Ref. [48] proposed a method to realize a perfect asymmetric blockade by dressing several Rydberg states with a strong microwave field, which provides strong theoretical support for future implementation of our scheme. As an example, we consider the fan-out gates performing X , T , and $X^{1/2}$ operations on the target qubits, which are called FOX, FOT, and FOX $^{1/2}$ in the following. In contrast to the previous works in Refs. [47,93], our proposed scheme has the following distinguished features. First, our proposed scheme can implement arbitrary single-qubit operations (other than a NOT or phase operation) on the target atoms. Second, the shortest evolution path to the target atoms can be found by introducing the time-optimal control (TOC) technology [94–98], based on which the shortest duration time can be acquired. Third, with the geometric phase involved, our scheme is less sensitive to the relative errors of Rabi frequency and detuning induced by imperfect operations.

The article is organized as follows. In Sec. II we present the theoretical framework of the geometric quantum fan-out gates, which is achieved by introducing the optimal control technique and geometric phase. Section III describes the performance and robustness of our quantum fan-out gates, an experimental problem is considered, and a numerical simulation is done based on the parameters available in experiment. In addition, we briefly describe the application of the fan-out gate in the entangled state preparation. A brief summary is given in Sec. IV. Mathematical details can be found in Appendices A and B.

II. RYDBERG GEOMETRIC FAN-OUT GATE WITH TOC

As sketched in Fig. 1, we show the relevant energy levels of N atoms for realizing the Rydberg quantum gate, where our scheme consists of one control atom (red) labeled 1 and $N - 1$ target qubits (green) labeled 2, 3, 4, \dots , N , respectively. In such an available two-dimensional (2D) atom array [99], the

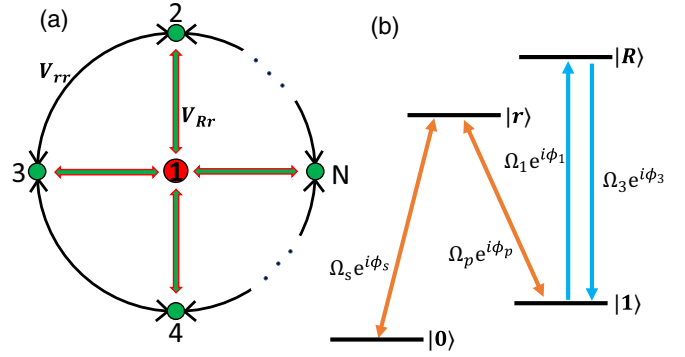


FIG. 1. Illustration of the implementation of the geometric fan-out gate. (a) Schematic diagram with the control atom (red) labeled 1 and multiple target atoms (green) labeled 2, 3, 4, \dots , N . (b) Coupling configuration. For atom 1, state $|1\rangle$ is resonantly coupled to the Rydberg $|R\rangle$ with Rabi frequency $\Omega_1(t)$ [$\Omega_3(t)$] and phase $\phi_1(t)$ [$\phi_3(t)$] in step (i) [(iii)]. For qubit 2 or 3, the ground states $|0\rangle$ and $|1\rangle$ are resonantly coupled to the Rydberg state $|r\rangle$ with the Rabi frequencies $\Omega_s(t)e^{i\phi_s(t)}$ and $\Omega_p(t)e^{i\phi_p(t)}$ in step (ii).

target atoms sit on a ring and the control atom is located in the center, which ensures equivalent control-target interactions. The qubit basis states are represented by a pair of long-lived hyperfine ground-state sublevels $|0\rangle$ and $|1\rangle$ which can be manipulated by a microwave field or an optical Raman transition. The ground state $|1\rangle$ of the control atom can be resonantly coupled to the Rydberg state $|R\rangle$ by focusing the laser field with Rabi frequency $\Omega_1(t)e^{i\phi_1(t)}$ in step (i) and $\Omega_3(t)e^{i\phi_3(t)}$ in step (iii) [$\Omega_{1(3)}(t)$ and $\phi_{1(3)}(t)$ are the maximum value and phase of the Rabi frequency, respectively]; two external classical fields are necessary for the target atoms to resonantly drive the atomic transition $|0\rangle \leftrightarrow |r\rangle$ with $\Omega_s(t)e^{i\phi_s(t)}$ and $|1\rangle \leftrightarrow |r\rangle$ with $\Omega_p(t)e^{i\phi_p(t)}$ in step (ii). In our scheme, the Rydberg-Rydberg interactions have two forms, i.e., the dipole-dipole (DD) interaction and the vdW interaction. The control-target interaction is a DD interaction with strength V_{Rr} coupling near resonant product states $|R, r\rangle_{j,j'} \equiv |R\rangle_j \otimes |r\rangle_{j'}$ and $|r, R\rangle_{j,j'}$, whereas the target-target interaction is a vdW interaction with strength V_{rr} resonantly coupling product states $|r, r\rangle_{j,j'}$ and $|r, r\rangle_{j,j'}$ (the subscripts represent different atoms). We will introduce our nontrivial geometric fan-out gates based on the unconventional geometric phase, NHQC, and the asymmetric Rydberg blockade $V_{Rr} \gg \Omega_{s(p)} \gg V_{rr}$, which has no requirement for the Rabi frequency of the control qubit.

A. Three-qubit fan-out gate

We consider three four-level Rydberg atoms including one control atom (atom 1) and two target atoms (atoms 2 and 3). The construction of the geometric fan-out gate requires the three following steps.

Step (i). Turn on the laser on the control atom with the Hamiltonian

$$\mathcal{H}_1(t) = \frac{\Omega_1(t)}{2} e^{i\phi_1} |1\rangle_1 \langle R| + \text{H.c.}, \quad (1)$$

where H.c. denotes Hermitian conjugate (here and throughout we set $\hbar \equiv 1$). Apply a π pulse on the control atom with initial phase ϕ_1 in the process of the first step; then the transition $|1\rangle \rightarrow |R\rangle$ is achieved when atom 1 is in state $|1\rangle$. Assuming $\Omega_1(t)$ in step (i) is constant, labeled Ω_0 , then the gating time of the first step is $\tau_1 = \pi/\Omega_0$. State $|0\rangle$ is completely decoupled from the lasers due to the transition selection rule or large transition frequency mismatch augmented by properly shaped laser pulses.

Step (ii). Turn off the laser on atom 1 and turn on the lasers on the target atoms 2 and 3 with identical Rabi frequencies and phases. The RRI Hamiltonian among the three atoms can be expressed as

$$\mathcal{H}_v = \sum_{j=2}^3 (V_{Rr}|Rr\rangle_{1j}\langle rR| + \text{H.c.}) + V_{rr}|rr\rangle_{23}\langle rr|. \quad (2)$$

In addition, with the condition of $\Omega_{s(p)}(t) \gg V_{rr}$, atoms 2 and 3 can be simultaneously excited to the Rydberg state $|r\rangle$ due to the small energy shift induced by V_{rr} with respect to the Rabi frequency $\Omega_{s(p)}(t)$ [8]. Thus, the interactions between the three atoms are reduced to two two-body interactions only existing between the control atom 1 and the target atom 2 (3) because the interaction between atoms 2 and 3 can be ignored. Now let us turn our attention to the dynamics between atoms 1 and 2, which is identical to the dynamics between atoms 1 and 3. The Hamiltonian of atom 2 can be written as

$$\mathcal{H}_2(t) = \frac{\Omega_s(t)}{2} e^{i\phi_s(t)} |0\rangle_2 \langle r| + \frac{\Omega_p(t)}{2} e^{i\phi_p(t)} |1\rangle_2 \langle r| + \text{H.c.} \quad (3)$$

In addition, the RRI Hamiltonian

$$\mathcal{H}_v^{1,2}(t) = V_{Rr}|Rr\rangle_{12}\langle rR| + \text{H.c.} \quad (4)$$

is relevant to Rydberg blockade depending on whether the control atom is excited or not. Thus the two-atom conditional dynamics are described in Figs. 2(b) and 2(c), with the former showing the dynamics of the control atom in state $|0\rangle$ and the latter the dynamics of the control atom in state $|1\rangle$. The effective Hamiltonian in Fig. 2(b) is given by

$$\mathcal{H}_{e1} = \frac{\Omega_s(t)}{2} e^{i\phi_s(t)} |00\rangle \langle 0r| + \frac{\Omega_p(t)}{2} e^{i\phi_p(t)} |01\rangle \langle 0r| + \text{H.c.} \quad (5)$$

Here and throughout we omit the subscripts for simplicity. By setting $\phi = \phi_s(t) - \phi_p(t)$, $\Omega_s(t) = \sqrt{\Omega_s^2(t) + \Omega_p^2(t)} \sin(\theta/2)$, and $\Omega_p(t) = \sqrt{\Omega_s^2(t) + \Omega_p^2(t)} \cos(\theta/2)$, with θ and ϕ constant values, Eq. (5) can be reexpressed as

$$\mathcal{H}_{e1} = \frac{\sqrt{\Omega_s^2(t) + \Omega_p^2(t)}}{2} e^{i\phi_p(t)} |b\rangle \langle 0r| + \text{H.c.}, \quad (6)$$

where the bright state $|b\rangle = \sin(\theta/2)e^{i\phi}|00\rangle + \cos(\theta/2)|01\rangle$. Thus, only states $|b\rangle$ and $|0r\rangle$ are resonantly coupled with Rabi frequency $\sqrt{\Omega_s^2(t) + \Omega_p^2(t)}$, i.e., the dynamics of the quantum system are captured by the resonant coupling between the bright state $|b\rangle$ and $|0r\rangle$, while the dark eigenstate $|d\rangle =$

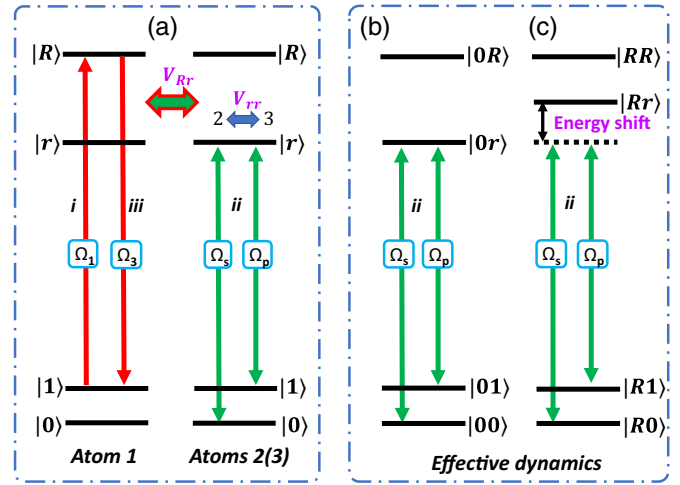


FIG. 2. (a) Pulse sequence of the three-qubit fan-out gate based on asymmetric Rydberg blockade. The effective dynamical process of step (ii) in the two-atom basis is shown (b) without and (c) with RRI. With the control atom 1 not excited to $|R\rangle$, all target atoms undergo the same resonance evolution. However, with the control atom excited to $|R\rangle$, the resonance condition is broken due to an energy shift V_{Rr} of the Rydberg state $|r\rangle$ induced by DD interaction, thereby leading to off-resonant Raman transfer from $|0\rangle$ to $|1\rangle$ on target atoms. The concrete energy-level structure will be described in Sec. III.

$\cos(\theta/2)|00\rangle - \sin(\theta/2)e^{-i\phi}|01\rangle$ is left unchanged. Note that the effective Rabi frequency $\sqrt{\Omega_s^2(t) + \Omega_p^2(t)}$ does not originate from additional fields. Similarly, the effective Hamiltonian in Fig. 2(c) can be calculated as

$$\mathcal{H}_{e2} = \frac{\Omega_s(t)\Omega_p(t)}{4V_{Rr}} e^{i\phi} |R0\rangle \langle R1| + \text{H.c.} \quad (7)$$

Considering the condition $V_{Rr} \gg \Omega_{s(p)}(t)$, in the timescale of resonance dynamics in Fig. 2(b), the off-resonant dynamics in Fig. 2(c) only leads to a rotation by a very small angle from the initial state. Namely, there is no effective dynamics going on in Fig. 2(c), because the energy shift V_{Rr} of the DD interaction induced by the Rydberg state $|r\rangle$ is much larger than the Rabi frequency of the target atom, preventing quantum jumps from $|0\rangle$ and $|1\rangle$ to the Rydberg state $|r\rangle$. This is known as the Rydberg blockade [8]. Note that the level shifts induced by the vdW interaction and DD interaction are the result of a pairwise interaction. Finally, the effective dynamics of the two-atom quantum system can be described by the Hamiltonian (6).

Without a loss of generality, we select a set of basis vectors $\{|\psi_0(t)\rangle, |\psi_1(t)\rangle, |\psi_2(t)\rangle\}$ as

$$\begin{aligned} |\psi_0\rangle &= (c_{\eta_1/2} - is_{\eta_1/2})e^{i\eta_2/2}|0r\rangle - is_{\eta_3}s_{\eta_1/2}e^{-i\eta_2/2}|b\rangle, \\ |\psi_1\rangle &= -is_{\eta_3}s_{\eta_1/2}e^{i\eta_2/2}|0r\rangle + (c_{\eta_1/2} + is_{\eta_1/2}c_{\eta_3})e^{-i\eta_2/2}|b\rangle, \\ |\psi_2\rangle &= |d\rangle, \end{aligned} \quad (8)$$

which follows the time-dependent Schrödinger equation (TDSE) $i|\dot{\psi}_k(t)\rangle = \mathcal{H}(t)|\psi_k(t)\rangle$ [$\mathcal{H}(t) = \mathcal{H}_{e1}$ for simplicity], with $\{\eta_1, \eta_2, \eta_3\}$ the parameters defined, $s_x = \sin x$, $c_x = \cos x$, and η_3 a constant (η_1 and η_2 are

time dependent). By directly substituting the parameters into the TDSE, the control parameters of pulses, namely, the Rabi frequency $\sqrt{\Omega_s^2(t) + \Omega_p^2(t)}$ and phase $\phi_p(t)$, must satisfy the parameter relations $\sqrt{\Omega_s^2(t) + \Omega_p^2(t)} = \eta_1'(t) \sin \eta_3$ and $\phi_p(t) = \eta_2(t)$. To this end, the time-evolution operator can be expressed as

$$\mathcal{U}(t) = \mathcal{T} \exp\left(-i \int_0^t \mathcal{H}(t') dt'\right) = \sum_{m=0}^2 |\psi_m(t)\rangle \langle \psi_m(0)|, \quad (9)$$

which shows that transitions from the state $|\psi(t)\rangle$ to its orthogonal states will not occur during the whole quantum evolution governed by the Hamiltonian $\mathcal{H}(t)$.

For the realization of the scheme, to guarantee pure geometric properties of fan-out gates, we need to eliminate the accumulation of the dynamical phase, thus satisfying an unconventional geometric condition [100]. We introduce a set of auxiliary bases $\{|\mu_m(t)\rangle\}$ defined by $|\mu_0(t)\rangle = e^{-i\lambda_1(t)}|\psi_0\rangle$, $|\mu_1(t)\rangle = e^{i\lambda_1(t)}|\psi_1\rangle$, and $|\mu_2(t)\rangle = |\psi_2\rangle$, with $\lambda_1(0) = 0$, which does not need to satisfy the TDSE. If the cyclic evolution conditions are satisfied [$\eta_1(\tau) = 2\pi$], namely, $|\mu_m(\tau)\rangle = |\mu_m(0)\rangle = |\psi_m(\tau)\rangle$, the unitary transformation matrix at the final time τ of step (ii) can be expressed as $\mathcal{U}(\tau) = \sum_{lm} \{\mathcal{T} \exp[i \int (A + K) dt]\}_{lm} |\psi_l(0)\rangle \langle \psi_m(0)|$, where the dynamical and geometric parts are $K_{ml} = -\langle \mu_m(t) | \mathcal{H}(t) | \mu_l(t) \rangle$ and $A_{ml} = i \langle \mu_m(t) | \frac{d}{dt} | \mu_l(t) \rangle$, respectively. However, the existence of the dynamical phase $\int K dt$ will damage the geometric noise-resilient feature.

In contrast to simply eliminating the dynamic phase as in NHQC schemes [76,77], which will inevitably limit the geometric gating time and weaken the robustness of the geometric gate, we adopt a special approach to deal with it. Using Eq. (9), the geometric parts can be obtained as $A_{ml} = A_{ml}^\lambda + A_{ml}^\eta$, where $A_{ml}^\lambda = \sum_a i \langle \mu_m | \frac{\partial}{\partial \eta_a} | \mu_l \rangle (\frac{d\eta_a}{dt})$ and $A_{ml}^\eta = \sum_b i \langle \mu_m | \frac{\partial}{\partial \eta_b} | \mu_l \rangle (\frac{d\eta_b}{dt})$, and we have $K_{ml} + A_{ml}^\eta = 0$. Consequently, the global phase generated during this evolution is purely geometric because the dynamical phase has been offset, i.e., the geometric phase $\gamma = \int A_{ml}^\lambda dt$. Thus, at the final time of step (ii), the evolution operator can be expressed as

$$\mathcal{U}_1 = e^{i\gamma} |\mu_1(0)\rangle \langle \mu_1(0)| + |\mu_2(0)\rangle \langle \mu_2(0)| \quad (10)$$

in the computational subspace $\{|\mu_1(0)\rangle, |\mu_2(0)\rangle\}$, where $\gamma = \lambda_1(\tau) - \pi + \eta_2(\tau_1 + \tau_2)/2$ is a pure geometric phase. Within the logic subspace $\{|0\rangle, |1\rangle\}$, when atom 1 is initially in state $|0\rangle$, this evolution operator is equivalent to a controlled single-qubit operation

$$\mathcal{U}(\theta, \phi, \gamma) = e^{i(\gamma/2)} e^{-i(\gamma/2)(\vec{n} \cdot \vec{\sigma})}, \quad (11)$$

where $\vec{\sigma} = (\sigma_x, \sigma_y, \sigma_z)$ are the standard Pauli operators, $\vec{n} = (\sin \theta \cos \phi, -\sin \theta \sin \phi, \cos \theta)$ is a unit vector, and $e^{-i(\gamma/2)(\vec{n} \cdot \vec{\sigma})}$ conducts a rotation around \vec{n} by an arbitrary γ . That is, if atom 1 is initially in state $|0\rangle$, target atom 2 can gain a pure geometric phase, i.e., any desired single-qubit geometric gate of target qubits can be realized via the proper choice of θ , ϕ , and γ .

Furthermore, the main obstacle to the realization of high-fidelity quantum gates is the error caused by either inaccurate manipulation of the quantum system or interaction with

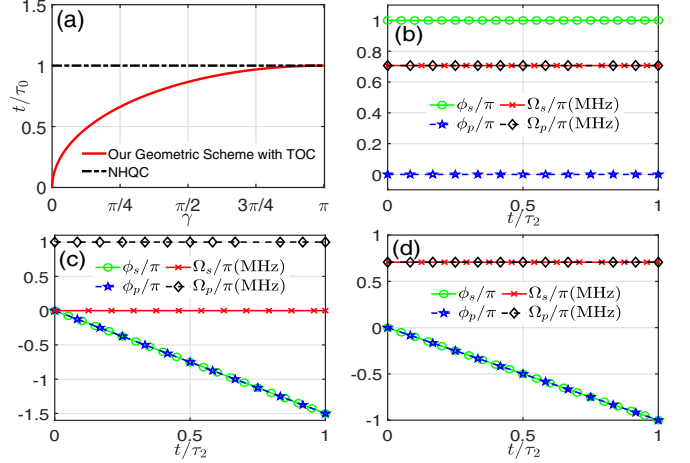


FIG. 3. (a) Comparison of the gating time for the NHQC in Refs. [76,77,83] and our geometric scheme with TOC. The phases ϕ_s and ϕ_p and Rabi frequencies Ω_s and Ω_p of the target atom vary in time τ_2 in step (ii) for the geometric (b) FOX gate, (c) FOT gate, and (d) FOX^{1/2} gate.

the environment. Therefore, to further pursue higher gate fidelity and stronger robustness, one possible measure is to reduce the decoherence effects by minimizing the gating time. Here we incorporate the TOC technique [94,96–98,101] into our framework of quantum computation. We can simply set $\sqrt{\Omega_s^2(t) + \Omega_p^2(t)} = 2\pi \times 1$ MHz (different gates have different Ω_s and Ω_p , but the ratios of Ω_s and Ω_p are fixed). The engineering of the Hamiltonian $\mathcal{H}(t)$ needs to satisfy the following constraints: (i) The Rabi frequency of the microwave field cannot be infinite, i.e., $l_1[\mathcal{H}(t)] = \frac{1}{2}[\text{Tr}[\mathcal{H}^2(t)] - \frac{1}{2}\Omega_0^2] = 0$, and (ii) the Hamiltonian of a realistic quantum device usually takes a given form, i.e., $l_2[\mathcal{H}(t)] = \text{Tr}[\mathcal{H}(t)\sigma_z'] = 0$ (σ_z' is the Pauli operator in the subspace of $\{|b\rangle, |0r\rangle\}$), so only a limited quantum trajectory can be realized. Furthermore, by solving the quantum brachistochrone equation [94] $i\partial F/\partial t = [\mathcal{H}(t), F]$, where $F = \partial L_c/\partial \mathcal{H}(t)$ and $L_c = \sum_i \mu_i f_i(\mathcal{H}(t))$, with μ_i the Lagrange multiplier, the parameters of the laser field are determined by

$$\phi_p(t) = \eta_2(t) = 2(\gamma - \pi)(t - \tau_1)/\tau_2, \quad (12)$$

realizing the minimum evolution time in step (ii), $\tau_2 = 2\sqrt{\pi^2 - (\pi - \gamma)^2}/\Omega_0$, which clearly shows that the gating time of target qubits can be greatly reduced compared with NHQC with gating time $\tau_0 = 2\pi/\Omega_0$, especially at small angles of rotation as shown in Fig. 3(a). Thus, we have shown how to implement the fan-out gate geometrically, which improves NHQC by efficiently reducing its gate time and strengthening its robustness.

Next we can construct the unconventional nonadiabatic geometric operations using similar pulses because the effective Hamiltonian between atoms 1 and 3 is similar to Eq. (6). When step (ii) is finished, we acquire the evolution operator

$$\mathcal{U}' = |0\rangle \langle 0| \otimes \mathcal{U}(\theta, \phi, \gamma) \otimes \mathcal{U}(\theta, \phi, \gamma) + |R\rangle \langle R| \otimes \mathcal{I}_2 \otimes \mathcal{I}_2, \quad (13)$$

where $\mathcal{I}_2 = |0\rangle \langle 0| + |1\rangle \langle 1|$.

Step (iii). Turn off the laser applied to the target atoms and turn on lasers on the control atom with duration $\tau_3 = \pi/\Omega_0$. Applying a π pulse with phase $\phi_3 = \phi_1 + \pi$ turns the control atom from the Rydberg state $|R\rangle$ to the state $|1\rangle$ without additional phase accumulation. The evolution operator in the whole evolution process can therefore be expressed as

$$\mathcal{U}_f = |0\rangle\langle 0| \otimes \mathcal{U}(\theta, \phi, \gamma) \otimes \mathcal{U}(\theta, \phi, \gamma) + |1\rangle\langle 1| \otimes \mathcal{I}_2 \otimes \mathcal{I}_2. \quad (14)$$

After completing the above three steps, we achieve the quantum controlled gates with arbitrary single quantum operations. For example, the three-qubit geometric gates FOX, FOT, and FOX^{1/2} can be realized, respectively, by choosing the parameters

$$\begin{aligned} \theta &= \pi/2, & \phi &= \pi, & \gamma &= \pi & \text{for } X, \\ \theta &= 0, & \phi &= 0, & \gamma &= \pi/4 & \text{for } T, \\ \theta &= \pi/2, & \phi &= 0, & \gamma &= \pi/2 & \text{for } X^{1/2}, \end{aligned} \quad (15)$$

which represent nontrivial geometric fan-out gates.

Note that the parameters $\{\theta, \phi, \gamma\}$ can be implemented by fixing $\{\Omega_s(t)/\Omega_p(t), \phi_s(t) - \phi_p(t), -\pi + \phi_p(\tau_1 + \tau_2)/2\}$, respectively. Figures 3(b)–3(d) describe the parameters $\{\phi_s(t), \phi_p(t), \Omega_s(t), \Omega_p(t)\}$ of a single target atom varying in τ_2 for different gates of the target qubits [here, for convenience, we set the beginning of step (ii) or the end of step (i) as time zero]. Additionally, the only requirement for steps (i) and (iii) is that there is a π phase difference between steps (i) and (iii).

B. Nontrivial multiqubit fan-out gate

We extend our scheme to the multiqubit case without increasing the total operation time, which is important for quantum computers due to the lack of resources for full fault tolerance. The process for executing such a geometric fan-out gate also follows three steps. The first and third steps are the same as in the case of three atoms; the only differences are in step (ii). In this case, Eqs. (1) and (4) remain invariant, but the RRI Hamiltonian should be updated to ($j < j'$)

$$\mathcal{H}_v = \sum_{j=2}^N \left(V_{Rr} |Rr\rangle_{1j} \langle rR| + \text{H.c.} + \sum_{j'}^N V_{rr} |rr\rangle_{jj'} \langle rr| \right). \quad (16)$$

After considering the asymmetric RRI, since $\Omega_0 \gg V_{rr}$, the interactions among the target atoms do not affect the evolutions. Nevertheless, the state of the control atom will influence the evolution of target atoms due to the condition $V_{Rr} \gg \Omega_0$, and the Rydberg blockade emerges if the control atom is initially in state $|1\rangle$. Thus, after accomplishing the above three steps, the multiqubit geometric fan-out gates

$$\mathcal{U}_f = |0\rangle\langle 0| \otimes \mathcal{U}^{\otimes N-1} + |1\rangle\langle 1| \otimes \mathcal{I}_2^{\otimes N-1}, \quad (17)$$

where one control qubit and multiple target qubits can be achieved, with $\mathcal{U}^{\otimes N-1} = \frac{\mathcal{U} \otimes \mathcal{U} \otimes \dots \otimes \mathcal{U}}{N-1}$ and $\mathcal{I}_2^{\otimes N-1} = \frac{\mathcal{I}_2 \otimes \mathcal{I}_2 \otimes \dots \otimes \mathcal{I}_2}{N-1}$.

C. Composite scheme

To realize arbitrary controlled operations with better suppression versus parameter fluctuation, we can use the method of composite pulses. Similar to the conventional composite-pulse scheme [87,102], in this case, the whole evolution of the second step is also divided into two segments and the phase $\phi_p(t)$ of $\mathcal{H}_2(t)$ has the form

$$\begin{aligned} \phi_p(t) &= 2(\gamma/2 - \pi)(t - \tau_1)/t', & t &\in (\tau_1, \tau_1 + t'], \\ \phi_p(t) &= \pi + 2(\gamma/2 - \pi)(t - \tau_1)/t', & t &\in (\tau_1 + t', \tau_1 + 2t'], \end{aligned} \quad (18)$$

where $t' = 2\sqrt{\pi^2 - (\pi - \gamma/2)^2}/\Omega_0$ is the time in each segment. The corresponding evolution operators are

$$\begin{aligned} \mathcal{U}_{c1} &= e^{i\gamma/2} |\mu_1(0)\rangle \langle \mu_1(0)| + |\mu_2(0)\rangle \langle \mu_2(0)|, \\ \mathcal{U}_{c2} &= -e^{i\gamma/2} |\mu_1(0)\rangle \langle \mu_1(0)| - |\mu_2(0)\rangle \langle \mu_2(0)|. \end{aligned} \quad (19)$$

Then the final evolution operator can be obtained as

$$\mathcal{U}_c = \mathcal{U}_{c2} \mathcal{U}_{c1} = \mathcal{U}_1, \quad (20)$$

which forms two loops in the Grassmannian $\mathcal{G}\{4; 2\}$, i.e., the space of two-dimensional subspaces of a four-dimensional Hilbert space, and each of the two segments has a complete circle of evolution on the Bloch sphere.

III. DISCUSSION

In this section, taking the three-qubit FOT and FOX gates as two examples, we first compare the gate performance of our geometric scheme with its dynamical counterpart against environment-induced decoherence (dynamical schemes can be found in Appendix B). Then the effect of an imperfect asymmetric blockade and the relative errors of parameters on FOT and FOX gates are also discussed. An experimental example is also briefly described. Finally, we briefly describe how to implement the Greenberger-Horne-Zeilinger (GHZ) state based on the FOX gate.

A. Gate performance and robustness

In the above sections, we demonstrated how to realize the multiqubit geometric fan-out gates. Our scheme can greatly reduce the fan-out gating time, which is independent of the qubit number. Here we focus on several factors relevant to the performance of our quantum gates. One is the spontaneous emission from the high-lying Rydberg state and the other is the blockade error. In addition, we will prove the superiority of the geometric phase, i.e., robustness to the noisy environment. In particular, the composite-pulse scheme can further improve robustness. In our simulations, we set $w = V_{Rr}/\Omega_0$ and $q = \Omega_0/V_{rr}$, where w and q are blockade coefficients. The method for calculating the average fidelity is given in Appendix A.

As shown in Fig. 4, we plot the effect of the atomic spontaneous rate of the control and target atoms on the average fidelities of the three-qubit FOT gate. The results show that the geometric FOT gate has a higher fidelity and a smaller reduction than the dynamical FOT gate for identical blockade coefficients. In particular, the geometric scheme with an imperfect Rydberg blockade can perform better than the

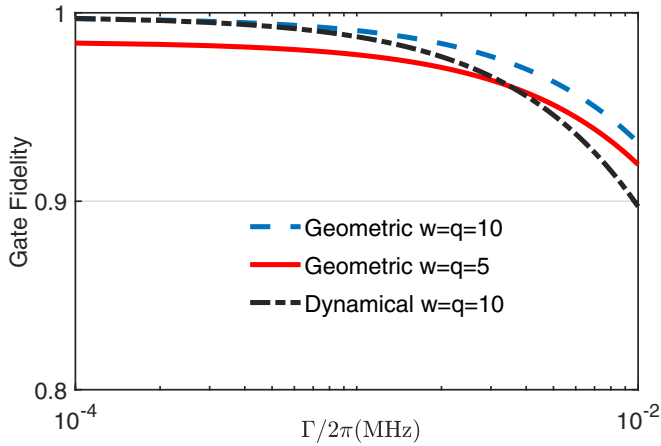


FIG. 4. Average fidelities of the three-qubit FOT gate versus atomic spontaneous rate Γ for geometric and dynamical FOT gates with different block coefficients w and q .

dynamical scheme with a perfect Rydberg blockade when the spontaneous emission rates of the atoms are much larger.

The second factor is the error caused by an imperfect blockade. As discussed earlier, one of the key points for the geometric fan-out gate is to keep the asymmetric blockade effect valid. However, if perfect asymmetric RRI is not strictly met, it would be challenging to execute the Rydberg blockade and the collective excitation of multiple target atoms. In order to demonstrate the superiority of the proposed geometric fan-out gate, we plot the average fidelities of the three-qubit FOX and FOT gates versus different blockade coefficients w and q in Fig. 5. The results indicate that the proposed geometric fan-out gate is less sensitive to the change of blockade coefficient than the dynamical scheme. In other words, when the conditions $V_{Rr} \gg \Omega_0 \gg V_{rr}$ are not strictly satisfied, our geometric solution is still a good choice. It is necessary to emphasize that the reason for the high fidelity in an imperfect blockade is

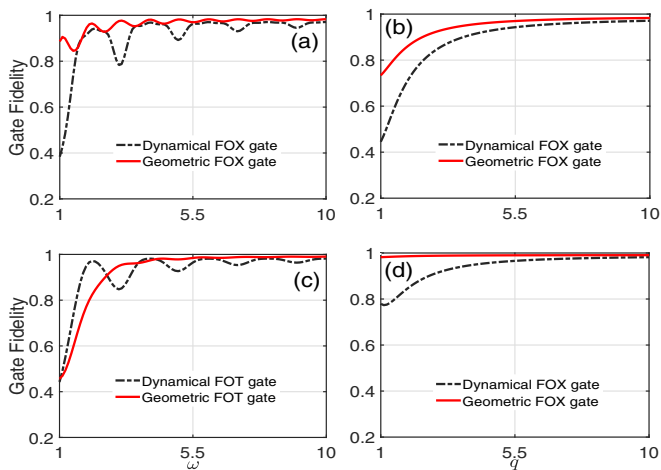


FIG. 5. Performance of FOX and FOT gates under imperfect Rydberg blockade based on different schemes, i.e., geometric and dynamical schemes, for (a) and (c) $q = 10$ and (b) and (d) $w = 10$. Here all the atomic spontaneous rates of the Rydberg atoms are the same, i.e., $\Gamma = 1$ kHz.

the peculiarity of the FOT gate. Note that the ground state $|0\rangle$ is decoupled from the Rydberg state in our scheme, i.e., $\Omega_s = 0$ MHz in the construction of the FOT gate (for the FOX gate, $\Omega_s = \Omega_p \neq 0$). We start from eight initial states of the three qubits $\{|000\rangle, |010\rangle, |001\rangle, |011\rangle, \dots\}$ and the corresponding ideal states $\{|000\rangle, e^{i\pi/4}|010\rangle, e^{i\pi/4}|001\rangle, e^{i\pi/2}|011\rangle, \dots\}$, based on which we can find that the vdW interaction mainly affects the evolution process of the initial state $|011\rangle$. Thus, although the ratio q is too small to satisfy the asymmetric blockade condition, the reason for such high fidelities of the FOT gate in Fig. 5(d) is that each component's weight is identical in calculating the average fidelities of the FOT gate, namely, V_{rr} only has a small impact on the average fidelity of the FOT gate. In addition, we want to point out that this particular example does not mean that our scheme can work outside the asymmetric blockade condition.

In addition, the imperfect operations have considerable impact on the dynamical phase generated during the whole evolution, since small fluctuations in the Hamiltonian are fed back into the evolution operator immediately. Fortunately, the introduction of geometric phases can help us suppress the adverse effects from the relative fluctuation of laser parameters and enhance robustness. The Rabi-frequency error will occur when the strength of the driving field deviates from the ideal value by an unknown fraction. In addition, the error in frequency detuning appears when the laser is not exactly resonant with the atomic transition, which will break the resonant conditions and induce an off-resonant evolution. Thus, for both the qubit frequency drift δ and the relative error of Rabi frequency ϵ in the form of $\Delta\Omega_0/\Omega_0$ leading to $\mathcal{H}_1(t) \rightarrow \mathcal{H}'_1(t) = (1 + \epsilon)\Omega_1(t)/2e^{i\phi_1}|1\rangle_1\langle R| + \text{H.c.} + \delta|R\rangle_1\langle R|$ and $\mathcal{H}_2(t) \rightarrow \mathcal{H}'_2(t) = (1 + \epsilon)\Omega_s(t)/2e^{i\phi_s(t)}|0\rangle_2\langle r| + (1 + \epsilon)\Omega_p(t)/2e^{i\phi_p(t)}|1\rangle_2\langle r| + \text{H.c.} + \delta|r\rangle_2\langle r|$, we plot the average fidelity of the three-qubit FOT gate based on geometric and dynamical schemes, which show that our implemented geometric gate is more noise resilient than the dynamical scheme and the composite scheme further improves robustness as shown in Fig. 6.

B. Experimental consideration

We know that the performance of the proposed scheme depends on the strength of the blockade interactions and the degree to which the couplings are asymmetric. For a concrete experimental process, here we consider the excitation from the ground state to the Rydberg state achieved by a two-photon process or single-photon process in a Rb atom platform, with the ground state encoding $|0\rangle = |5S_{1/2}, F = 1, m_F = -1\rangle$ and $|1\rangle = |5S_{1/2}, F = 1, m_F = 1\rangle$. According to recent work [48], by dressing several Rydberg states $|s\rangle = |60S_{1/2}, m_j = 1/2\rangle$, $|p_0\rangle = |60P_{1/2}, m_j = 1/2\rangle$, and $|p_+\rangle = |59P_{1/2}, m_j = -1/2\rangle$ with strong microwave fields (with different polarizations), the dressed states $|R\rangle$ and $|r\rangle$ can be achieved with theoretically estimated lifetimes of 356 and 431 μs and the correspond decay rates $\Gamma_R = 2.80$ kHz and $\Gamma_r = 2.32$ kHz, respectively. Theoretical prediction of the interaction gives $C_3 = -2\pi \times 730$ MHz μm^3 and $C_6 = 2\pi \times 600$ MHz μm^6 [48], based on which the minimum control-target dipole-dipole interactions can be calculated as $V_{Rr} =$

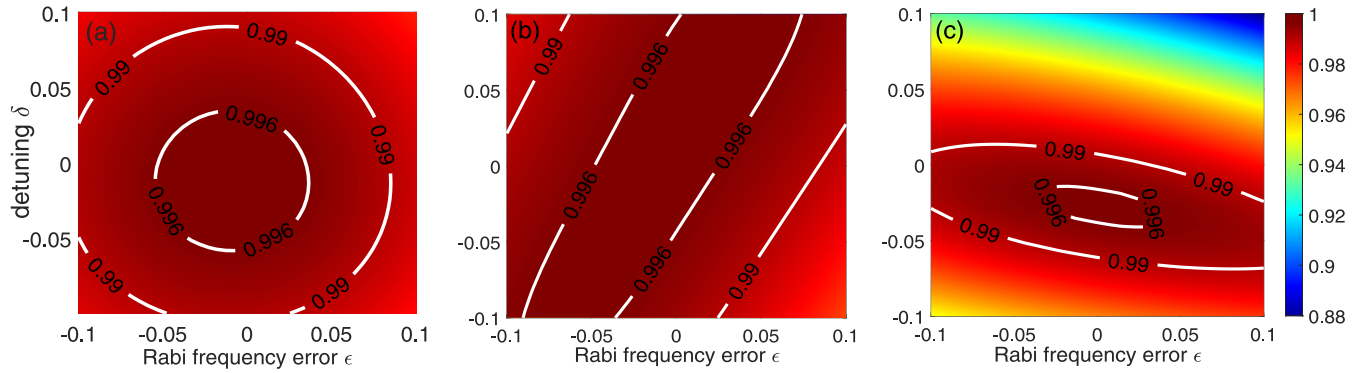


FIG. 6. Average fidelities of the three-qubit FOT gate for the (a) geometric, (b) composite, and (c) dynamical schemes for the Rabi frequency error ϵ and off-resonance error δ in the form of $\Delta\Omega_0/\Omega_0$. Here we set $V_{Rr} = 2\pi \times 10$ MHz, $V_{rr} = 2\pi \times 0.1$ MHz, and $\Gamma = 0$.

$-2\pi \times 12.55$ MHz and the maximum target-target vdW interactions are $V_{rr} = -2\pi \times 0.13$ MHz by choosing the radius of the ring $d_1 = 2.1 \mu\text{m}$ and the nearest-neighbor separation of the target atoms $d_2 = 3 \mu\text{m}$, respectively. In addition, in order to satisfy the asymmetric Rydberg blockade, we set the Rabi frequencies of target atoms $\Omega_0 = 2\pi \times 1.3$ MHz and control atom $\Omega_1(t) = \Omega_3(t) = 2\pi \times 12$ MHz. Note that the parameters selected above can be easily obtained and adjusted experimentally [26,103,104]. In the case of three-qubit gates in Fig. 7(b), our thorough numerical calculations indicate that the gate fidelity can reach 99.51% for the geometric FOT gate and 98.73% for the geometric FOX gate as shown in Figs. 7(c) and 7(d), respectively. In addition, as our proposed gate implementation scheme partially relies on the phase relations between different excitations as shown in Fig. 3, it is interesting to see how much fluctuations in the relative phases between the fields would affect gate performance. Here we only consider the effects of relative phase fluctuations of target atoms. As shown in Fig. 7(e), we plot the average fidelities as a function of relative phase error in the form of $[-0.1\pi, 0.1\pi]$, which shows that our scheme still has good robustness.

There is no obstacle to the realization of such a setting with the current experimental technique. The defect-free atomic 2D array with a ring geometry in Fig. 1(a) can be readily achieved in current experiments [14,19,99], and recent experiments [104–108] have demonstrated the possibility of building an atomic array with such nearest-neighbor separation. We mention that, although one can place maximally $N = 4$ atoms on the 2D ring, the defect-free 3D array in Fig. 7(a) with the target atoms distributed on a spherical surface may also be accessible [108–110], from which the available number of target atoms can be greatly increased.

Recently, the addressing and manipulation of a single qubit in 2D and 3D arrays have made remarkable progress experimentally [17–19,28,103,104,111], and it is possible to confine a single ^{87}Rb atom in optical traps with a $1\text{-}\mu\text{m}$ waist or even smaller [104,111]. These achievements have greatly advanced the applications using neutral-atom systems in quantum simulation and quantum computation. Thus our proposed scheme is feasible in experiments. Additionally, the target atoms can be driven by $N - 1$ independent fields with different driving parameters by using a single-site addressing technique and thus different single-site quantum operations can be performed.

C. Application of the fan-out gate

The proposed geometric fan-out gates can be widely used in quantum algorithms [112] and the preparation of

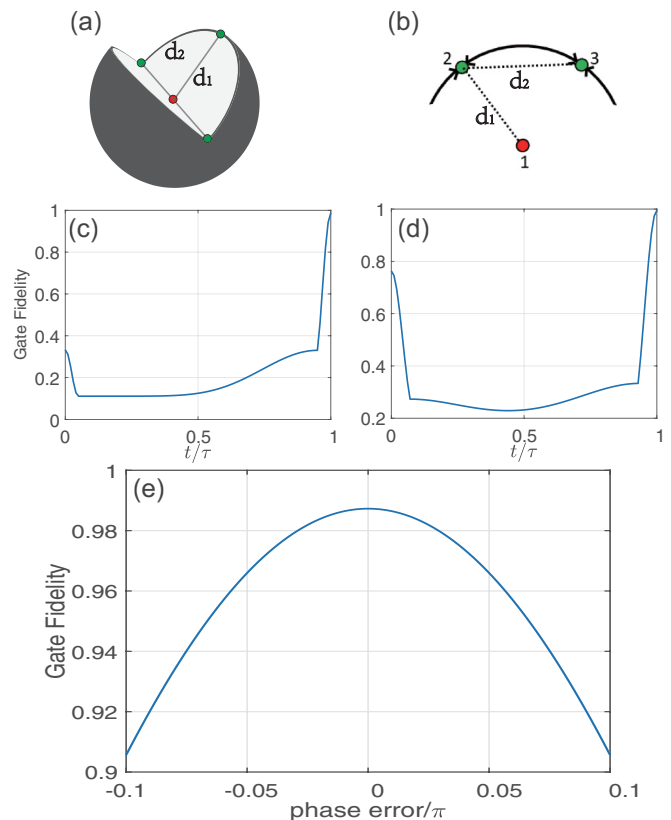


FIG. 7. Rydberg atom setting and dynamics of the three-qubit FOT gate. (a) Extended 3D view. (b) Spatial configuration of the three-Rydberg-atom array. The fidelities of three-qubit geometric gates, that is, the (c) FOT and (d) FOX gates, are shown as functions of the evolution time when the control atom is located at the center of the circle. (e) Gate performance of the FOX gate under phase fluctuation for the range of $[-0.1\pi, 0.1\pi]$. The spontaneous emission rate of the dressed Rydberg state $|R\rangle$ ($|r\rangle$) is 2.80 (2.32) kHz. The dipole-dipole interaction $V_{Rr} = -2\pi \times 12.55$ MHz, the Rabi frequency of the target atoms $\Omega_0 = 2\pi \times 1.3$ MHz, and the vdW interaction $V_{rr} = -2\pi \times 0.13$ MHz.

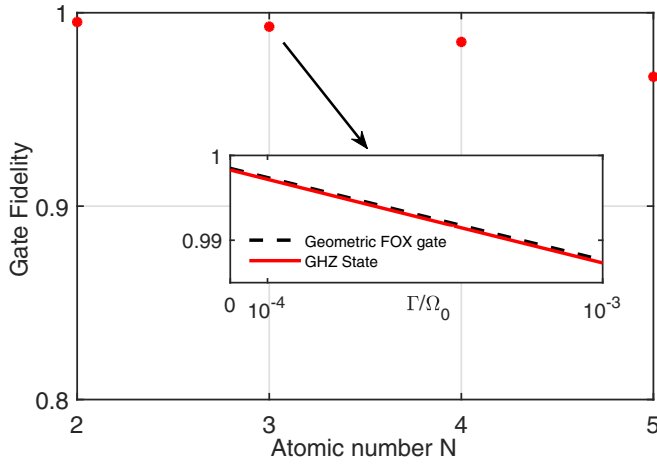


FIG. 8. Variation trends of the GHZ state fidelity versus the number of qubits. The inset shows $|\text{GHZ}\rangle_3 = (|000\rangle + |111\rangle)/\sqrt{2}$ and the three-qubit FOX gate versus the rate of decay Γ . The other parameters are $\Gamma = \Omega_0/1000$, $V_{Rr} = 10\Omega_0$, and $V_{rr} = \Omega_0/10$ in our simulations.

the entanglement state [45]. Here we take the N -particle Greenberger-Horne-Zeilinger state

$$|\text{GHZ}_N\rangle = \frac{1}{\sqrt{2}}(|0101\dots\rangle + |1010\dots\rangle) \quad (21)$$

as a typical example. Such a state provides an important resource for applications that range from quantum metrology [113,114] to quantum error correction [44]. Therefore, the preparation of a multipartite GHZ state is particularly important.

The GHZ state preparation protocol is as follows. Initially, all atoms are in state $|1\rangle$ except for a single atom in state $(|0\rangle + |1\rangle)/\sqrt{2}$. This single atom will be the control atom, while the $N - 1$ nearest neighbors are target atoms. A geometric FOX gate is applied, creating a many-body entangled state

$$\frac{|0\rangle + |1\rangle}{\sqrt{2}} \otimes |1\dots 1\rangle \xrightarrow{\text{FOX}} \frac{|00\dots 0\rangle + |11\dots 1\rangle}{\sqrt{2}}, \quad (22)$$

which is one of the GHZ states. The performance of the geometric FOX gate can be evaluated by generating an N -atom GHZ state $|\text{GHZ}\rangle_N = (\frac{|00\dots 0\rangle}{N} + \frac{|11\dots 1\rangle}{N})/\sqrt{2}$ from an initial state $|\psi_i\rangle = (\frac{|01\dots 1\rangle}{N} + \frac{|11\dots 1\rangle}{N})/\sqrt{2}$. In Fig. 8 we plot the GHZ state fidelity up to five atoms by numerically solving the TDSE [the fidelity is defined as $\mathcal{F} = \langle \text{GHZ} | \rho(t) | \text{GHZ} \rangle$], which shows that GHZ states induced by the geometric FOX gate have high fidelities even in the presence of large dissipation.

IV. CONCLUSION

Using the asymmetric Rydberg-Rydberg interaction, time-optimal control technology, and an unconventional geometric phase, we have proposed and analyzed a geometric scheme of the fan-out gate with one control and multiple target qubits that can be performed with arbitrary operations. The Rydberg blockade being proved experimentally [90,91] and the

asymmetric Rydberg-Rydberg interaction being predicted theoretically [47,48] ensure the feasibility of the physical model of our scheme. Geometric quantum computation and optimal control technology provide the technical feasibility of the scheme and its advantages over using other Rydberg atoms to construct fan-out gates. Our scheme not only maintains the superiority of the geometric phase but greatly reduces the gating time. By numerically simulating the average fidelity of the geometric FOX or FOT gate and dynamical counterparts under spontaneous emission, the relative error of the Rabi frequency, the off-resonance error, the phase error, and an imperfect blockade, we prove that our gate scheme indeed has a better performance and higher fidelity than the three-qubit dynamical controlled gate scheme. Thus, our scheme provides a promising way towards fault-tolerant quantum computation of a neutral-atom-based system.

ACKNOWLEDGMENTS

This work was supported by Special Project for Research and Development in Key Fields of Guangdong Province under Grant No. 2020B0303300001, by National Key Research and Development Program of China under Grant No. 2017YFA0304503, by National Natural Science Foundation of China under Grants No. 12074346, No. 12074390, No. 11835011, No. 11804375, No. 11804308, No. 91421111, and No. 11734018, by Natural Science Foundation of Henan Province under Grants No. 202300410481 and No. 212300410085, and by K. C. Wong Education Foundation (Grant No. GJTD-2019-15).

APPENDIX A: MASTER EQUATION AND AVERAGE FIDELITY

In a practical implementation of the fan-out gate, we need to consider the spontaneous emission of Rydberg atoms. Generally speaking, the quantum dynamics of the whole system described by the Hamiltonian \mathcal{H} can be described by the master equation

$$\dot{\rho} = -i[\mathcal{H}, \rho] + \frac{\Gamma}{2} \sum_{j=1}^N \left[\sum_{a=4j-3}^{4j} (2\sigma_a \rho \sigma_a^\dagger - \sigma_a^\dagger \sigma_a \rho - \rho \sigma_a^\dagger \sigma_a) \right], \quad (\text{A1})$$

where H denotes the Hamiltonian of the system, Γ is the decay rate of the Rydberg atoms, and $\sigma_{4j-3} = |0\rangle_j \langle R|$, $\sigma_{4j-2} = |1\rangle_j \langle R|$, $\sigma_{4j-1} = |0\rangle_j \langle r|$, and $\sigma_{4j} = |1\rangle_j \langle r|$ are the four decay channels of the j th atom. To evaluate the performance of the fan-out gate, we introduce the trace-preserving quantum-operator-based average fidelity [115,116] defined as

$$\bar{\mathcal{F}}(\zeta, \mathcal{K}) = \frac{\sum_j \text{tr}[\mathcal{K} \mathcal{K}_j^\dagger \mathcal{K}_j^\dagger \zeta(\mathcal{K}_j)] + b^2}{b^2(b+1)}, \quad (\text{A2})$$

where \mathcal{K}_j is the tensor of Pauli matrices $\frac{\mathcal{I}_2 \mathcal{I}_2 \dots \mathcal{I}_2 \mathcal{I}_2}{N}$, $\frac{\mathcal{I}_2 \mathcal{I}_2 \dots \mathcal{I}_2 \sigma_y}{N}$, \dots , $\frac{\mathcal{I}_2 \mathcal{I}_2 \dots \sigma_x \mathcal{I}_2}{N}$, $\frac{\mathcal{I}_2 \mathcal{I}_2 \dots \sigma_x \sigma_y}{N}$, \dots , $\frac{\sigma_z \sigma_z \dots \sigma_z \sigma_y}{N}$, $\frac{\sigma_z \sigma_z \dots \sigma_z \sigma_z}{N}$ for the N -qubit quantum gates, \mathcal{K} is the ideal fan-out gate, $b = 2^N$, and ζ is the trace-preserving quantum operator.

APPENDIX B: DYNAMICAL SCHEME

Here we briefly explain the dynamical scheme mentioned in the main text to achieve FOX and FOT gates. Taking a three-qubit gate as an example, the process can be divided into three similar steps.

Step (i) is the same as the geometric scheme.

In step (ii) we set $\Omega_s = 0$ for the rest of the Rydberg atoms 2 and 3. In the interaction picture, the interaction Hamiltonian of this system is

$$\mathcal{H}_d = \sum_{j=2}^3 \frac{\Omega_p}{2} e^{i\phi_p} |1\rangle_j \langle r| + \text{H.c.} \quad (\text{B1})$$

With this Hamiltonian we can obtain an evolution operator similar to the geometric gate

$$\mathcal{U}_d = \begin{pmatrix} 1 & 0 & 0 \\ 0 & \cos \beta & -ie^{i\phi_p} \sin \beta \\ 0 & -ie^{-i\phi_p} \sin \beta & \cos \beta \end{pmatrix}, \quad (\text{B2})$$

where $\beta = \Omega_p \tau / 2$, with τ the gate duration. During this evolution, which is divided into two parts to acquire T gates on target atoms, the parameters of the Hamiltonian are chosen as

$$\begin{aligned} \beta &= \pi/2, & \phi_p &= 3\pi/8, & t &\in [t_1, t_1 + t'_2/2], \\ \beta &= \pi/2, & \phi_p &= -3\pi/8, & t &\in [t_1 + t'_2/2, t_1 + t'_2], \end{aligned} \quad (\text{B3})$$

where $t'_2 = 2\pi/\Omega_p$ is the whole gating time in step (ii). Thus, the evolution operators of target atoms 2 and 3 in computation subspace ($|0\rangle, |1\rangle$) are all T gates. Suppose the conditions

$V_{Rr} \gg \Omega_p \gg V_{rr}$ are satisfied. Then the transition $|\alpha\beta\rangle_{23} \rightarrow (e^{i\pi/4})^\alpha (e^{i\pi/4})^\beta |\alpha\beta\rangle$ is achieved if the initial state of atom 1 is $|0\rangle$, where $\alpha, \beta \in 0, 1$. Otherwise, if the initial state of atom 1 is $|1\rangle$, then it would be excited to $|R\rangle$ after step (i). Thus, the transition $|\alpha\beta\rangle_{23} \rightarrow |\alpha\beta\rangle_{23}$ is achieved under an asymmetric Rydberg blockade.

Step (iii) is also the same as the geometric scheme. Thus, we can acquire the whole evolution process

$$\begin{aligned} |0\alpha\beta\rangle &\rightarrow (e^{i\pi/4})^\alpha (e^{i\pi/4})^\beta |0\alpha\beta\rangle, \\ |1\alpha\beta\rangle &\rightarrow |1\alpha\beta\rangle, \end{aligned} \quad (\text{B4})$$

which represents the three-qubit FOT gate. Additionally, the dynamical FOX gate can also be achieved. In step (ii) we divide the total evolution time $3\pi/\Omega_0$ into three equal parts π/Ω_0 , and each part of the Hamiltonian can be represented as

$$\begin{aligned} \mathcal{H}_{d1} &= \sum_{j=2}^3 \frac{\Omega_s}{2} e^{i\phi_s} |0\rangle_j \langle r| + \text{H.c.}, & \phi_s &= 0, \\ \mathcal{H}_{d2} &= \sum_{j=2}^3 \frac{\Omega_p}{2} e^{i\phi_s} |1\rangle_j \langle r| + \text{H.c.}, & \phi_p &= \pi, \\ \mathcal{H}_{d3} &= \sum_{j=2}^3 \frac{\Omega_s}{2} e^{i\phi_s} |0\rangle_j \langle r| + \text{H.c.}, & \phi_s &= 0, \end{aligned} \quad (\text{B5})$$

respectively. Thus, the dynamical FOX gate can be realized at the end of the evolution.

-
- [1] G. K. Brennen, C. M. Caves, P. S. Jessen, and I. H. Deutsch, *Phys. Rev. Lett.* **82**, 1060 (1999).
- [2] D. S. Weiss and M. Saffman, *Phys. Today* **70**(7), 44 (2017).
- [3] T. F. Gallagher, *Rydberg Atoms* (Cambridge University Press, Cambridge, 1994).
- [4] C. S. Adams, J. D. Pritchard, and J. P. Shaffer, *J. Phys. B* **53**, 012002 (2019).
- [5] M. Saffman, I. I. Beterov, A. Dalal, E. J. Pérez, and B. C. Sanders, *Phys. Rev. A* **101**, 062309 (2020).
- [6] F. Robicheaux, T. M. Graham, and M. Saffman, *Phys. Rev. A* **103**, 022424 (2021).
- [7] T. M. Wintermantel, Y. Wang, G. Lochead, S. Shevate, G. K. Brennen, and S. Whitlock, *Phys. Rev. Lett.* **124**, 070503 (2020).
- [8] D. Jaksch, J. I. Cirac, P. Zoller, S. L. Rolston, R. Côté, and M. D. Lukin, *Phys. Rev. Lett.* **85**, 2208 (2000).
- [9] W. Li and I. Lesanovsky, *Appl. Phys. B* **114**, 37 (2014).
- [10] D. Comparat and P. Pillet, *J. Opt. Soc. Am. B* **27**, A208 (2010).
- [11] S.-L. Su, F.-Q. Guo, L. Tian, X.-Y. Zhu, L.-L. Yan, E.-J. Liang, and M. Feng, *Phys. Rev. A* **101**, 012347 (2020).
- [12] M. D. Lukin, M. Fleischhauer, R. Cote, L. M. Duan, D. Jaksch, J. I. Cirac, and P. Zoller, *Phys. Rev. Lett.* **87**, 037901 (2001).
- [13] L. Béguin, A. Vernier, R. Chicireanu, T. Lahaye, and A. Browaeys, *Phys. Rev. Lett.* **110**, 263201 (2013).
- [14] M. Saffman, T. G. Walker, and K. Mølmer, *Rev. Mod. Phys.* **82**, 2313 (2010).
- [15] D. Schrader, I. Dotsenko, M. Khudaverdyan, Y. Miroshnychenko, A. Rauschenbeutel, and D. Meschede, *Phys. Rev. Lett.* **93**, 150501 (2004).
- [16] S. Olmschenk, R. Chicireanu, K. D. Nelson, and J. V. Porto, *New J. Phys.* **12**, 113007 (2010).
- [17] T. Xia, M. Lichtman, K. Maller, A. W. Carr, M. J. Piotrowicz, L. Isenhower, and M. Saffman, *Phys. Rev. Lett.* **114**, 100503 (2015).
- [18] Y. Wang, X. Zhang, T. A. Corcovilos, A. Kumar, and D. S. Weiss, *Phys. Rev. Lett.* **115**, 043003 (2015).
- [19] Y. Wang, A. Kumar, T.-Y. Wu, and D. S. Weiss, *Science* **352**, 1562 (2016).
- [20] J. H. Lee, E. Montano, I. H. Deutsch, and P. S. Jessen, *Nat. Commun.* **4**, 2027 (2013).
- [21] A. Smith, B. E. Anderson, H. Sosa-Martinez, C. A. Riofrío, I. H. Deutsch, and P. S. Jessen, *Phys. Rev. Lett.* **111**, 170502 (2013).
- [22] L. Isenhower, E. Urban, X. L. Zhang, A. T. Gill, T. Henage, T. A. Johnson, T. G. Walker, and M. Saffman, *Phys. Rev. Lett.* **104**, 010503 (2010).
- [23] T. Wilk, A. Gaëtan, C. Evellin, J. Wolters, Y. Miroshnychenko, P. Grangier, and A. Browaeys, *Phys. Rev. Lett.* **104**, 010502 (2010).
- [24] K. M. Maller, M. T. Lichtman, T. Xia, Y. Sun, M. J. Piotrowicz, A. W. Carr, L. Isenhower, and M. Saffman, *Phys. Rev. A* **92**, 022336 (2015).
- [25] C. J. Picken, R. Legaie, K. McDonnell, and J. D. Pritchard, *Quantum Sci. Technol.* **4**, 015011 (2018).

- [26] H. Levine, A. Keesling, A. Omran, H. Bernien, S. Schwartz, A. S. Zibrov, M. Endres, M. Greiner, V. Vuletić, and M. D. Lukin, *Phys. Rev. Lett.* **121**, 123603 (2018).
- [27] H. Levine, A. Keesling, G. Semeghini, A. Omran, T. T. Wang, S. Ebadi, H. Bernien, M. Greiner, V. Vuletić, H. Pichler, and M. D. Lukin, *Phys. Rev. Lett.* **123**, 170503 (2019).
- [28] T. M. Graham, M. Kwon, B. Grinkemeyer, Z. Marra, X. Jiang, M. T. Lichtman, Y. Sun, M. Ebert, and M. Saffman, *Phys. Rev. Lett.* **123**, 230501 (2019).
- [29] I. S. Madjarov, J. P. Covey, A. L. Shaw, J. Choi, A. Kale, A. Cooper, H. Pichler, V. Schkolnik, J. R. Williams, and M. Endres, *Nat. Phys.* **16**, 857 (2020).
- [30] M. Müller, I. Lesanovsky, H. Weimer, H. P. Büchler, and P. Zoller, *Phys. Rev. Lett.* **102**, 170502 (2009).
- [31] S. L. Su, *Chin. Phys. B* **27**, 110304 (2018).
- [32] S. L. Su, H. Z. Shen, E. Liang, and S. Zhang, *Phys. Rev. A* **98**, 032306 (2018).
- [33] M. Li, F.-Q. Guo, Z. Jin, L.-L. Yan, E.-J. Liang, and S.-L. Su, *Phys. Rev. A* **103**, 062607 (2021).
- [34] T. H. Xing, X. Wu, and G. F. Xu, *Phys. Rev. A* **101**, 012306 (2020).
- [35] C.-P. Yang, Y.-x. Liu, and F. Nori, *Phys. Rev. A* **81**, 062323 (2010) C.-P. Yang, S.-B. Zheng, and F. Nori, **82**, 062326 (2010) C.-P. Yang, Q.-P. Su, and J.-M. Liu, *ibid.* **86**, 024301 (2012). C.-P. Yang, Q.-P. Su, Y. Zhang, and F. Nori, *ibid.* **101**, 032329 (2020).
- [36] L. Isenhower, M. Saffman, and K. Mølmer, *Quantum Inf. Process.* **10**, 755 (2011).
- [37] S.-L. Su, Y. Gao, E. Liang, and S. Zhang, *Phys. Rev. A* **95**, 022319 (2017).
- [38] L. K. Grover, *Phys. Rev. Lett.* **80**, 4329 (1998).
- [39] P. Høyer and R. Špalek, *Theory Comput.* **1**, 81 (2005).
- [40] W. L. Yang, C. Y. Chen, and M. Feng, *Phys. Rev. A* **76**, 054301 (2007).
- [41] H.-D. Yin and X.-Q. Shao, *Opt. Lett.* **46**, 2541 (2021).
- [42] A. M. Steane, *Phys. Rev. Lett.* **77**, 793 (1996).
- [43] P. W. Shor, *Phys. Rev. A* **52**, R2493 (1995).
- [44] M. A. Nielsen and I. L. Chuang, *Quantum Computation and Quantum Information* (Cambridge University Press, Cambridge, 2000).
- [45] M. Šašura and V. Bužek, *Phys. Rev. A* **64**, 012305 (2001).
- [46] E. Brion, A. S. Mouritzen, and K. Mølmer, *Phys. Rev. A* **76**, 022334 (2007).
- [47] M. Saffman and K. Mølmer, *Phys. Rev. Lett.* **102**, 240502 (2009).
- [48] J. T. Young, P. Bienias, R. Belyansky, A. M. Kaufman, and A. V. Gorshkov, *Phys. Rev. Lett.* **127**, 120501 (2021).
- [49] H. Wu, X.-R. Huang, C.-S. Hu, Z.-B. Yang, and S.-B. Zheng, *Phys. Rev. A* **96**, 022321 (2017).
- [50] M. M. Müller, D. M. Reich, M. Murphy, H. Yuan, J. Vala, K. B. Whaley, T. Calarco, and C. P. Koch, *Phys. Rev. A* **84**, 042315 (2011).
- [51] D. D. Bhaktavatsala Rao and K. Mølmer, *Phys. Rev. A* **90**, 062319 (2014).
- [52] X.-F. Shi and T. A. B. Kennedy, *Phys. Rev. A* **95**, 043429 (2017).
- [53] D. Petrosyan and K. Mølmer, *Phys. Rev. Lett.* **113**, 123003 (2014).
- [54] P. Bohlouli-Zanjani, J. A. Petrus, and J. D. D. Martin, *Phys. Rev. Lett.* **98**, 203005 (2007).
- [55] D. B. Tretyakov, V. M. Entin, E. A. Yakshina, I. I. Beterov, C. Andreeva, and I. I. Ryabtsev, *Phys. Rev. A* **90**, 041403(R) (2014).
- [56] S. Sevinçli and T. Pohl, *New J. Phys.* **16**, 123036 (2014).
- [57] A. W. Glaetzle, M. Dalmonte, R. Nath, I. Roussochatzakis, R. Moessner, and P. Zoller, *Phys. Rev. X* **4**, 041037 (2014).
- [58] D. W. Booth, J. Isaacs, and M. Saffman, *Phys. Rev. A* **97**, 012515 (2018).
- [59] S. K. Kanungo, J. D. Whalen, Y. Lu, M. Yuan, S. Dasgupta, F. B. Dunning, K. R. A. Hazzard, and T. C. Killian, *Nat. Commun.* **13**, 972 (2022).
- [60] M. Khazali and K. Mølmer, *Phys. Rev. X* **10**, 021054 (2020).
- [61] D. X. Li and X. Q. Shao, *Phys. Rev. A* **98**, 062338 (2018).
- [62] G. De Chiara and G. M. Palma, *Phys. Rev. Lett.* **91**, 090404 (2003).
- [63] S.-L. Zhu and P. Zanardi, *Phys. Rev. A* **72**, 020301(R) (2005).
- [64] P. J. Leek, J. M. Fink, A. Blais, R. Bianchetti, M. Göppl, J. M. Gambetta, D. I. Schuster, L. Frunzio, R. J. Schoelkopf, and A. Wallraff, *Science* **318**, 1889 (2007).
- [65] P. Zanardi and M. Rasetti, *Phys. Lett. A* **264**, 94 (1999).
- [66] J. Pachos, P. Zanardi, and M. Rasetti, *Phys. Rev. A* **61**, 010305(R) (1999).
- [67] L.-M. Duan, J. I. Cirac, and P. Zoller, *Science* **292**, 1695 (2001).
- [68] J. A. Jones, V. Vedral, A. Ekert, and G. Castagnoli, *Nature (London)* **403**, 869 (2000).
- [69] M. V. Berry, *Proc. R. Soc. London Ser. A* **392**, 45 (1984).
- [70] F. Wilczek and A. Zee, *Phys. Rev. Lett.* **52**, 2111 (1984).
- [71] X.-B. Wang and M. Keiji, *Phys. Rev. Lett.* **87**, 097901 (2001).
- [72] S.-L. Zhu and Z. D. Wang, *Phys. Rev. Lett.* **89**, 097902 (2002).
- [73] P. Z. Zhao, X.-D. Cui, G. F. Xu, E. Sjöqvist, and D. M. Tong, *Phys. Rev. A* **96**, 052316 (2017).
- [74] T. Chen and Z.-Y. Xue, *Phys. Rev. Appl.* **10**, 054051 (2018).
- [75] Y. Aharonov and J. Anandan, *Phys. Rev. Lett.* **58**, 1593 (1987).
- [76] E. Sjöqvist, D. M. Tong, L. M. Andersson, B. Hessmo, M. Johansson, and K. Singh, *New J. Phys.* **14**, 103035 (2012).
- [77] G. F. Xu, J. Zhang, D. M. Tong, E. Sjöqvist, and L. C. Kwek, *Phys. Rev. Lett.* **109**, 170501 (2012).
- [78] J. Anandan, *Phys. Lett. A* **133**, 171 (1988).
- [79] B.-J. Liu, X.-K. Song, Z.-Y. Xue, X. Wang, and M.-H. Yung, *Phys. Rev. Lett.* **123**, 100501 (2019).
- [80] Z.-Y. Xue, F.-L. Gu, Z.-P. Hong, Z.-H. Yang, D.-W. Zhang, Y. Hu, and J. Q. You, *Phys. Rev. Appl.* **7**, 054022 (2017).
- [81] B.-J. Liu, S.-L. Su, and M.-H. Yung, *Phys. Rev. Research* **2**, 043130 (2020).
- [82] G. F. Xu, C. L. Liu, P. Z. Zhao, and D. M. Tong, *Phys. Rev. A* **92**, 052302 (2015).
- [83] E. Sjöqvist, *Phys. Lett. A* **380**, 65 (2016).
- [84] P. Z. Zhao, G. F. Xu, Q. M. Ding, E. Sjöqvist, and D. M. Tong, *Phys. Rev. A* **95**, 062310 (2017).
- [85] E. Herterich and E. Sjöqvist, *Phys. Rev. A* **94**, 052310 (2016).
- [86] Z.-P. Hong, B.-J. Liu, J.-Q. Cai, X.-D. Zhang, Y. Hu, Z. D. Wang, and Z.-Y. Xue, *Phys. Rev. A* **97**, 022332 (2018).
- [87] Z. Zhu, T. Chen, X. Yang, J. Bian, Z.-Y. Xue, and X. Peng, *Phys. Rev. Appl.* **12**, 024024 (2019).
- [88] T. Yan, B.-J. Liu, K. Xu, C. Song, S. Liu, Z. Zhang, H. Deng, Z. Yan, H. Rong, K. Huang, M.-H. Yung, Y. Chen, and D. Yu, *Phys. Rev. Lett.* **122**, 080501 (2019).

- [89] J. W. Zhang, L.-L. Yan, J. C. Li, G. Y. Ding, J. T. Bu, L. Chen, S.-L. Su, F. Zhou, and M. Feng, *Phys. Rev. Lett.* **127**, 030502 (2021).
- [90] E. Urban, T. A. Johnson, T. Henage, L. Isenhower, D. D. Yavuz, T. G. Walker, and M. Saffman, *Nat. Phys.* **5**, 110 (2009).
- [91] A. Gaëtan, Y. Miroshnychenko, T. Wilk, A. Chotia, M. Viteau, D. Comparat, P. Pillet, A. Browaeys, and P. Grangier, *Nat. Phys.* **5**, 115 (2009).
- [92] Z. Eldredge, Z.-X. Gong, J. T. Young, A. H. Moosavian, M. Foss-Feig, and A. V. Gorshkov, *Phys. Rev. Lett.* **119**, 170503 (2017).
- [93] H.-Z. Wu, Z.-B. Yang, and S.-B. Zheng, *Phys. Rev. A* **82**, 034307 (2010).
- [94] A. Carlini, A. Hosoya, T. Koike, and Y. Okudaira, *Phys. Rev. A* **75**, 042308 (2007).
- [95] S. J. Glaser, U. Boscain, T. Calarco, C. P. Koch, W. Köckenberger, R. Kosloff, I. Kuprov, B. Luy, S. Schirmer, T. Schulte-Herbrüggen, D. Sugny, and F. K. Wilhelm, *Eur. Phys. J. D* **69**, 279 (2015).
- [96] A. Carlini and T. Koike, *J. Phys. A: Math. Theor.* **46**, 045307 (2013).
- [97] X. Wang, M. Allegra, K. Jacobs, S. Lloyd, C. Lupo, and M. Mohseni, *Phys. Rev. Lett.* **114**, 170501 (2015).
- [98] J. Geng, Y. Wu, X. Wang, K. Xu, F. Shi, Y. Xie, X. Rong, and J. Du, *Phys. Rev. Lett.* **117**, 170501 (2016).
- [99] D. Bluvstein, A. Omran, H. Levine, A. Keesling, G. Semeghini, S. Ebadi, T. T. Wang, A. A. Michailidis, N. Maskara, W. W. Ho, S. Choi, M. Serbyn, M. Greiner, V. Vuletić, and M. D. Lukin, *Science* **371**, 1355 (2021).
- [100] S.-L. Zhu and Z. D. Wang, *Phys. Rev. Lett.* **91**, 187902 (2003).
- [101] T. Chen and Z.-Y. Xue, *Phys. Rev. Appl.* **14**, 064009 (2020).
- [102] G. F. Xu, P. Z. Zhao, T. H. Xing, E. Sjöqvist, and D. M. Tong, *Phys. Rev. A* **95**, 032311 (2017).
- [103] A. Omran, H. Levine, A. Keesling, G. Semeghini, T. T. Wang, S. Ebadi, H. Bernien, A. S. Zibrov, H. Pichler, S. Choi, J. Cui, M. Rossignolo, P. Rembold, S. Montangero, T. Calarco, M. Endres, M. Greiner, V. Vuletić, and M. D. Lukin, *Science* **365**, 570 (2019).
- [104] H. Labuhn, D. Barredo, S. Ravets, S. de Léséleuc, T. Macrì, T. Lahaye, and A. Browaeys, *Nature (London)* **534**, 667 (2016).
- [105] M. O. Brown, T. Thiele, C. Kiehl, T.-W. Hsu, and C. A. Regal, *Phys. Rev. X* **9**, 011057 (2019).
- [106] A. Glicenstein, G. Ferioli, L. Brossard, Y. R. P. Sortais, D. Barredo, F. Nogrette, I. Ferrier-Barbut, and A. Browaeys, *Phys. Rev. A* **103**, 043301 (2021).
- [107] R. Samajdar, W. W. Ho, H. Pichler, M. D. Lukin, and S. Sachdev, *Proc. Natl. Acad. Sci. USA* **118**, e2015785118 (2021).
- [108] D. Barredo, S. de Léséleuc, V. Lienhard, T. Lahaye, and A. Browaeys, *Science* **354**, 1021 (2016).
- [109] D. Barredo, V. Lienhard, S. de Léséleuc, T. Lahaye, and A. Browaeys, *Nature (London)* **561**, 79 (2018).
- [110] A. Kumar, T.-Y. Wu, F. Giraldo, and D. S. Weiss, *Nature (London)* **561**, 83 (2018).
- [111] H. Bernien, S. Schwartz, A. Keesling, H. Levine, A. Omran, H. Pichler, S. Choi, A. S. Zibrov, M. Endres, M. Greiner, V. Vuletić, and M. D. Lukin, *Nature (London)* **551**, 579 (2017).
- [112] W.-L. Chang and A. V. Vasilakos, *Fundamentals of Quantum Programming in IBM's Quantum Computers* (Springer, Berlin, 2021).
- [113] V. Giovannetti, S. Lloyd, and L. Maccone, *Science* **306**, 1330 (2004).
- [114] L. Pezzè, A. Smerzi, M. K. Oberthaler, R. Schmied, and P. Treutlein, *Rev. Mod. Phys.* **90**, 035005 (2018).
- [115] M. A. Nielsen, *Phys. Lett. A* **303**, 249 (2002).
- [116] A. G. White, A. Gilchrist, G. J. Pryde, J. L. O'Brien, M. J. Bremner, and N. K. Langford, *J. Opt. Soc. Am. B* **24**, 172 (2007).